Manufacturing Rev. **5**, 8 (2018)

https://doi.org/10.1051/mfreview/2018003

Manufacturing Review
Available online at:
https://mfr.edp-open.org

REVIEW OPEN ACCESS

Green chemistry solutions for sol–gel micro-encapsulation of phase change materials for high-temperature thermal energy storage

Maria Dolores Romero-Sanchez[1,2], Radu-Robert Piticescu[2,*], Adrian Mihail Motoc[2], Francisca Aran-Ais[1], and Albert Ioan Tudor[2]

[1] INESCOP, Centre for Technology and Innovation, Elda-Alicante, Spain
[2] National R&D Institute for Nonferrous and Rare Metals, 102 Biruintei Blvd, Pantelimon, Ilfov, Romania

Received: 15 November 2017 / Accepted: 18 January 2018

Abstract. $NaNO_3$ has been selected as phase change material (PCM) due to its convenient melting and crystallization temperatures for thermal energy storage (TES) in solar plants or recovering of waste heat in industrial processes. However, incorporation of PCMs and $NaNO_3$ in particular requires its protection (i.e. encapsulation) into containers or support materials to avoid incompatibility or chemical reaction with the media where incorporated (i.e. corrosion in metal storage tanks). As a novelty, in this study, microencapsulation of an inorganic salt has been carried out also using an inorganic compound (SiO_2) instead of the conventional polymeric shells used for organic microencapsulations and not suitable for high temperature applications (i.e. 300–500 °C). Thus, $NaNO_3$ has been microencapsulated by sol–gel technology using SiO_2 as shell material. Feasibility of the microparticles synthetized has been demonstrated by different experimental techniques in terms of TES capacity and thermal stability as well as durability through thermal cycles. The effectiveness of microencapsulated $NaNO_3$ as TES material depends on the core:shell ratio used for the synthesis and on the maximum temperature supported by $NaNO_3$ during use.

Keywords: thermal energy storage / microencapsulation / sol–gel / inorganic salt / phase change material / $NaNO_3$ / concentrated solar power

1 Introduction

Thermal energy storage (TES) using phase change materials (PCMs, for latent heat storage) is a key technology in improving efficiency of Concentrated Solar Power Plant (CSP) where solar heat can be stored for electricity production when sunlight is not available or to recover waste heat in industrial processes. However, the use of PCMs for TES is currently facing different problems, such as the lack of thermal stability of the energy storage materials, loss of effectiveness and/or serious corrosion problems when working at high temperatures (in this context, high temperature is considered when storage is performed between 120 and 600 °C) [1–3]. Therefore, incorporation of PCMs into TES systems requires its encapsulation into containers or support materials to avoid incompatibility or reactivity problems within the media where incorporated (i.e. corrosion in metal storage tanks).

Macro- (>1 mm) and microencapsulation (μm or nm particle size) procedures have been successfully developed and patented for low temperature PCMs (organic and inorganic materials), mainly using polymeric shells [4–9], which cannot be used for high temperature applications. There are also some literature and even TES pilot installations using macroencapsulated inorganic salts. Zn, $NaNO_3$, $MgCl_2$, and eutectic mixtures with melting temperatures higher than 300 °C have been encapsulated according to US2011/0259544 [10] using Ni or carbon and stainless steel materials in the form of cylinders as containers, with mm to cm size. Patent US2012/0055661 [11] addresses to the encapsulation of molten salt nitrates in metal tubes which are sealed off for permanent containment. Recently, a procedure has been patented (US 2015/0284616) [12] for the encapsulation of molten salts such as $NaNO_3$ or KNO_3. This method is based on the coating of the PCM pellet (27 mm size) with a flexible polymer followed by metal coating by electroless and electroplating processes (Ni, Cu, Zn, Zn-Fe alloys, etc.). Using electroplating method, other authors (Maruoka et al.) have obtained particles (3 mm diameter) with lead-nickel core-shell structure suitable for heat recovery of high

* e-mail: rpiticescu@imnr.ro

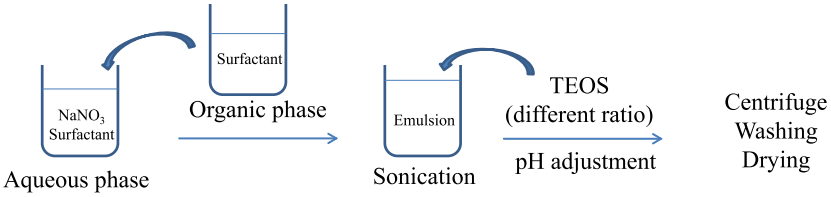

Scheme 1. Experimental procedure for $NaNO_3$-SiO_2 microparticles.

temperature waste heat [13]. More simple methods can also be used for the encapsulation of metal PCMs such as indium (melting temperature = 156 °C) by using silica as shell by sol–gel procedure and obtaining nm size particles [14]. However, this method requires the melting of the metal, with increased difficultness for handling when using metals with higher melting temperature. Authors have proposed sol–gel processes using organic polymers with high melting temperature (i.e. polyimide) and organic-inorganic hybrids shells for the microencapsulation of PCMs. In this sense, stainless steel has been coated by sol–gel procedure of hybrid coatings for corrosion protection with interesting results, forming a physical barrier towards corrosion [15,16]. However, although interesting studies have been carried out, neither suitable solutions for microencapsulation of inorganic PCMs in the range of 300–500 °C have been successfully encountered with the requirements for TES applications nor any product can be currently found in the market.

$NaNO_3$ has been identified in literature by several authors with thermal properties suitable for energy storage in CSP systems [17–22]. In this study, the objective is its microencapsulation using in situ synthetized SiO_2 shell by sol–gel procedure as a soft chemical synthesis procedure. Influence of $NaNO_3$ and SiO_2 precursors molar ratio on the TES capacity of microencapsulated $NaNO_3$ has been evaluated, as well as thermal stability through thermal cycles, as a method to evaluate the durability of synthetized materials and feasibility for TES [21].

2 Experimental

2.1 Materials and experimental procedure

Sodium nitrate salt ($NaNO_3$, 99.99% purity, Merck) has been selected as PCM to be microencapsulated, due to its convenient melting temperature for TES in CSP. $NaNO_3$ is water soluble (2 g/10 mL).

Sol–gel technique has been used for the microencapsulation of $NaNO_3$ into SiO_2 shells. Tetraethylorthosilicate (TEOS, Sigma-Aldrich) has been used as SiO_2 precursor.

Firstly, an aqueous phase containing hexadecyltrimethylammonium bromide (CTAB, Sigma-Aldrich) and $NaNO_3$ is prepared. An organic phase containing cyclohexane (CH, analysis grade, Merck) as solvent and Span 80 (Fluka) as surfactant is added drop by drop to the aqueous phase. An emulsion is obtained after vigorous stirring and sonication (2 min, 50% intensity, Branson Digital Sonication). Subsequently, corresponding amounts of TEOS ($NaNO_3$:SiO_2 molar ratio 1:0.5 and 1:0.25) are added drop by drop to the emulsion. NaOH 1 N was used to adjust pH to 11 for hydrolysis of TEOS to SiO_2 in alkaline media. After 12 h stirring, solution is twice centrifuged and washed with CH. Product obtained was dried in an oven at 40 °C for 24 h and subsequently at 150 °C for 24 h (Scheme 1).

2.2 Experimental techniques

Different experimental techniques have been used for the thermal, chemical and morphological characterization of the materials obtained.

2.2.1 Fourier Transform Infrared Spectroscopy (FT-IR)

It has been used to detect the chemical groups present in the particles and compared to the chemical composition of the raw materials.

The FT-IR spectra of the samples have been obtained using a Varian 660 FT-IR spectrophotometer (Varian, Inc.) with dry KBr pellets prepared using a manual hydraulic press. FT-IR spectra in absorbance mode were recorded (100 scans with 4 cm^{-1} resolution) among the range of 600–4000 cm^{-1}.

2.2.2 Scanning Electron Microscopy (SEM)

The surface morphology of the microparticles was obtained using a Phenom TM Electron Microscope system (SEM). For the SEM imaging, a drop of the corresponding microparticles dispersed in absolute ethanol was deposited on the sample holder and allowed to dry. The energy of the electron beam was 15 kV. This technique has been also used to estimate particle size. *Field emission scanning electron microscopy* (*FESEM*) has also been used for the characterization of morphology (Merlin VP Compact, Zeiss) working at higher resolution and reduced voltage (2 kV) minimizing charging effects.

2.2.3 Thermal Gravimetry Analysis (TGA)

TGA (TGA/Differential scanning calorimetry (DSC) 1 SF Star^e System, Mettler Toledo) has been used to evaluate thermal stability of the microparticles. Samples have been heated till 400 °C at 10 °C/min under N_2 atmosphere.

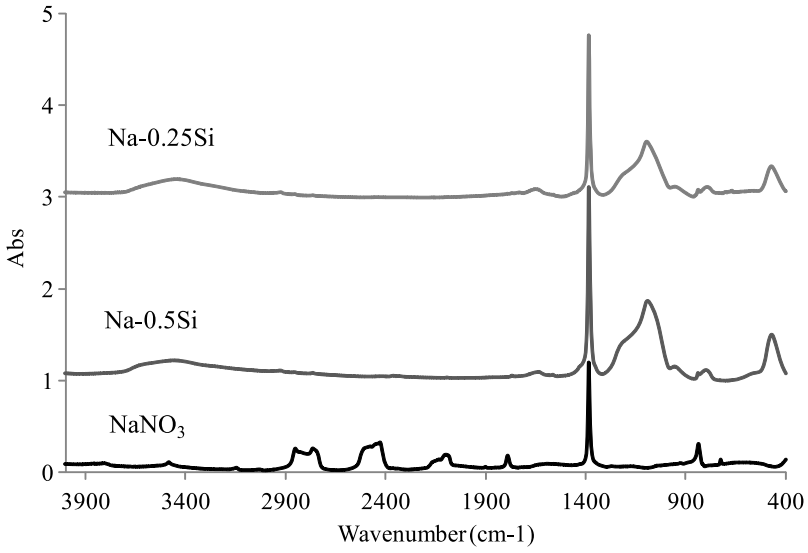

Fig. 1. FTIR spectra of $NaNO_3$ and synthetized Na-0.5Si and Na-0.25Si microparticles.

2.2.4 Differential Scanning Calorimetry (DSC)

Thermal properties of the microparticles obtained with the inorganic shell have been measured by using DSC. A DSC1/700 Star^e system, Mettler Toledo) Differential Scanning Calorimeter has been used at a heating rate of 10 °C/min among the range of 50–400 °C, with a sample weight of about 15 mg and under N_2 atmosphere.

Thermal analysis of the particles has been carried out during heating and cooling processes. Melting and crystallization temperatures and enthalpies have been calculated. Moreover, to evaluate thermal stability and durability of the microparticles, several thermal cycles have been carried out and melting and crystallization enthalpies have been calculated for comparison.

3 Results and discussion

$NaNO_3$-SiO_2 microparticles have been synthetized by sol–gel procedure using 1:0.5 and 1:0.25 molar ratios for $NaNO_3$:TEOS (as SiO_2 precursor), with the corresponding nomenclature Na-0.5Si and Na-0.25Si, respectively. The objective is to optimize this ratio to avoid the leakage of $NaNO_3$ when melted or the shielding of $NaNO_3$ by the SiO_2 shell losing heat storage capacity.

The analysis of the chemical composition of the synthetized Na-0.5Si and Na-0.25Si is shown in the IR spectra in Figure 1.

IR spectrum of $NaNO_3$ (Fig. 1) shows main peaks at 1385 cm^{-1} and 838 cm^{-1} due to N-O stretching vibration in NO_3^- and 2400–2500 cm^{-1} due to N = O stretching vibration.

IR spectra of samples Na-0.5Si and Na-0.25Si are very similar and show the characteristic bands of $NaNO_3$ at 1385 and 838 cm^{-1} (confirming the presence of nitrate) and the band at 1090 cm^{-1} ascribed to the Si-O bond in SiO_2. The band at 474 cm^{-1} may correspond to O-Si-O bending in SiO_2 and/or asymmetric and Si-O-Si bending vibrations of the SiO_2.

The band at 3440 cm^{-1} can be ascribed to the stretching vibration of O-H, Si-OH and/or N-H groups.

The presence of both compounds, $NaNO_3$ as PCM and SiO_2 as shell material have been identified in the FTIR spectra of the products synthetized, with different relative intensity of the typical bands for $NaNO_3$ and SiO_2 at 1385 and 1090 cm^{-1}, being higher for the Na-0.25Si microparticles (relative intensity = 2.88) compared to the Na-0.5Si microparticles (relative intensity = 2.37), indicating the higher proportion of SiO_2 in the Na-0.5Si sample. Moreover, this also indicates that the bonding between $NaNO_3$ and SiO_2 is a physical bonding. Other authors have previously obtained similar results when preparing mixed systems of $NaNO_3$ and $Sr(NO_3)_2$ single crystals in SiO_2 media [23].

The influence of the presence of SiO_2 on the thermal properties of $NaNO_3$ has been evaluated by DSC. Thermal properties of the samples synthetized have been analyzed during heating and cooling processes from 25 to 400 °C and 400 to 25 °C at 10 °C/min under N_2 atmosphere. Figure 2 includes the DSC thermogram for raw $NaNO_3$ used as PCM for microencapsulation. Melting and crystallization temperatures as well as the enthalpy of the respective processes (calculated by peak integration) have been included in Table 1. Values obtained for $NaNO_3$ agree with those obtained in literature [24,25] with some slight differences due to the different conditions used for the experiments (gas for atmosphere, heating and cooling speed rate, etc). Figure 2 shows two endothermic peaks for $NaNO_3$ during the heating process, at 278 °C due to a solid–solid phase transition and at 306.8 °C ascribed to the melting of $NaNO_3$ (melting enthalpy = 158.1 J/g). During the cooling process, an exothermic peak releasing the energy previously stored is observed at 304 °C and a solid phase transition at 270 °C. These values of thermal properties for $NaNO_3$ indicate the feasibility to be used as TES material. Figure 3 and Table 1 include the DSC thermograms and the quantified melting and crystallization temperatures (T_m, T_c) and enthalpies (ΔH_m, ΔH_c), respectively, for the samples Na-0.5Si and Na-0.25Si.

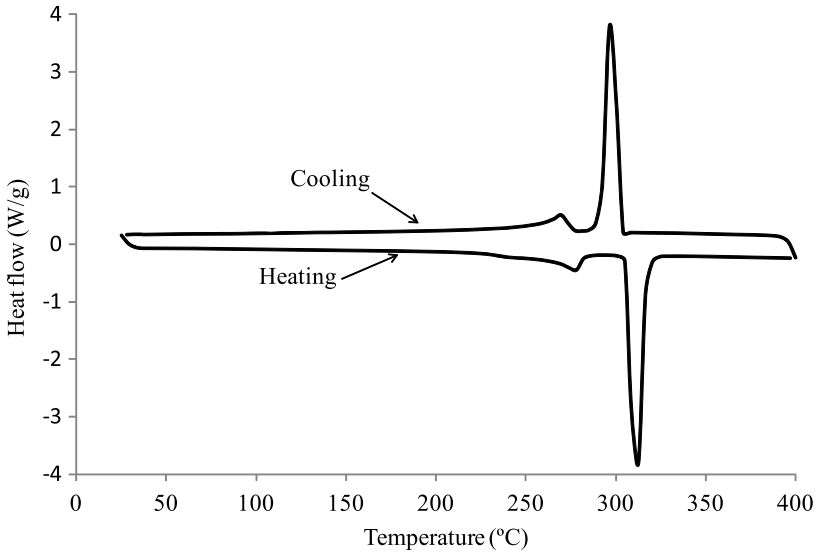

Fig. 2. DSC thermogram for $NaNO_3$.

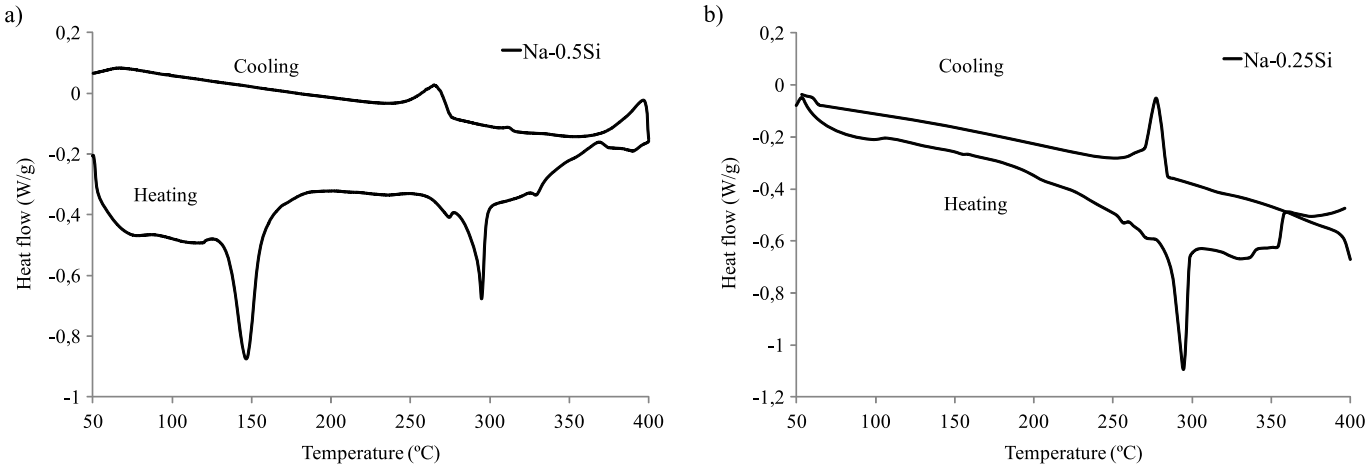

Fig. 3. DSC thermograms for (a) Na-0.5Si and (b) Na-0.25Si.

Table 1. Melting and cooling temperatures (T_m, T_c) and enthalpies (ΔH_m, ΔH_c) for raw $NaNO_3$ and Na-0.5Si and Na-0.25Si microparticles. Data obtained from DSC thermograms for heating and cooling processes.

Sample	Heating		Cooling	
	T_m (°C)	ΔH_m (J/g)	T_c (°C)	ΔH_c (J/g)
$NaNO_3$	306.8	158.1	304.0	159.4
Na-0.5Si	294.2	25.1	264.7	11.2
Na-0.25Si	293.4	29.0	277.5	21.0

As observed in Figure 3, the presence of SiO_2 produces some differences in the thermal behavior of synthetized Na-0.5Si and Na-0.25Si microparticles. In both cases, the melting temperature of $NaNO_3$ has decreased respect to the melting temperature in the raw $NaNO_3$. This could be explained because of the smaller particle size of the composites compared to the raw $NaNO_3$ and the fact that ΔH_m and ΔH_c (J/g) for the composites have been calculated including the SiO_2 weight [26–28].

Na-0.5Si microparticles show an endothermic peak at 146.0 °C, which may be due to impurities, as this peak does not appear when carrying out thermal cycles to Na-0.5Si microparticles and explained below.

On the other hand, the melting and cooling enthalpies of Na-0.5Si and Na-0.25Si microparticles are also affected by the presence of SiO_2, with a decrease in the crystallization temperature and enthalpy respect to the raw $NaNO_3$ due to the presence of the SiO_2 which is possible to restrict the crystallization of the $NaNO_3$ in the microparticles.

The microparticles prepared with the lower SiO_2 proportion (Na-0.25Si) show the highest melting and crystallization enthalpy values. The higher the enthalpy of this peak, the higher amount of energy stored.

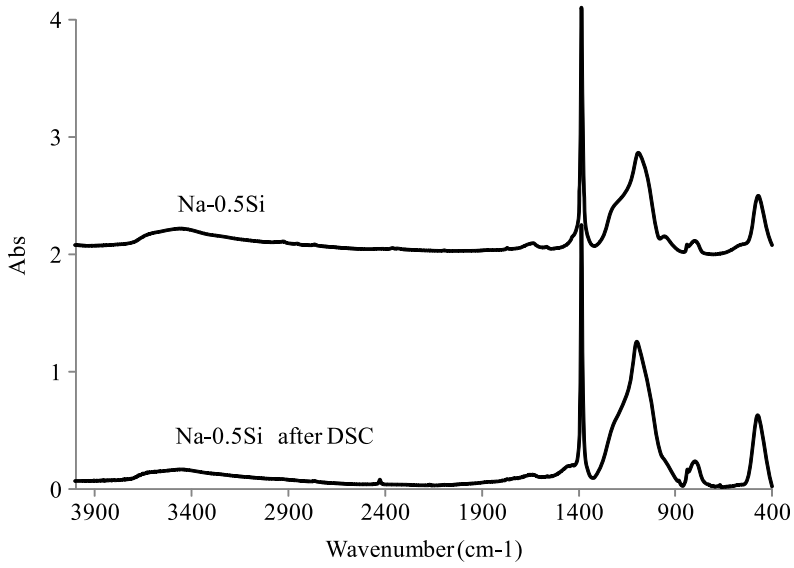

Fig. 4. FT-IR spectra of Na-0.5Si before and after DSC experiment.

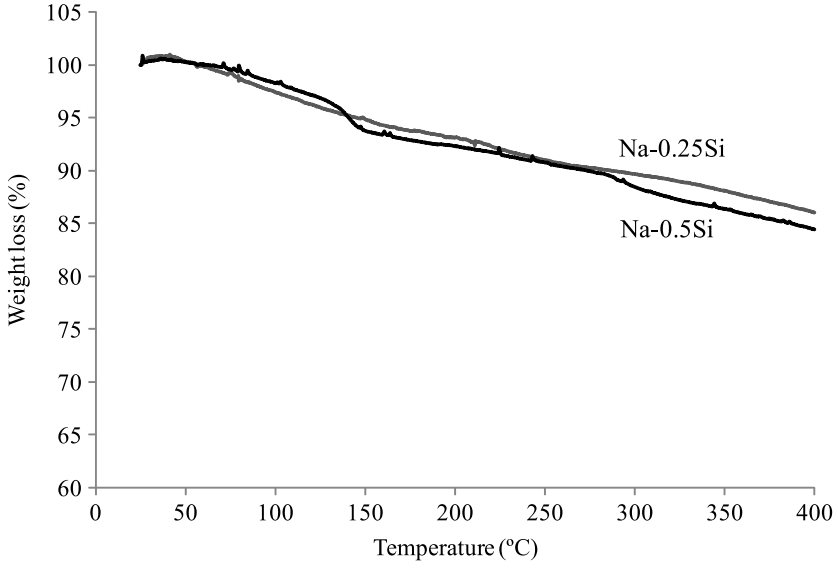

Fig. 5. TGA thermograms for raw $NaNO_3$ and Na-0.5Si and Na-0.25Si microparticles.

The effect of the heating and cooling process on the chemical composition of the microparticles has been evaluated by FTIR spectroscopy. Figure 4 includes the FTIR spectra of Na-0.5Si microparticles before and after DSC experiment.

Na-0.5Si microparticles after DSC experiment show similar bands in the FTIR spectrum as same microparticles before DSC. The typical band for the $NaNO_3$ appears at 1385 cm^{-1} and the Si-O band at 1090 cm^{-1}. However, the relative intensity of these bands changes after the heating and cooling process in the DSC experiment. Relative intensity values of 2.33 and 1.77 (relative intensity of the bands at 1385 and 1090 cm^{-1}) have been obtained for the microparticles of Na-0.5Si and Na-0.5Si after DSC, respectively, indicating a reduction of the $NaNO_3$ proportion respect to the SiO_2 in the Na-0.5Si microparticles after DSC experiment. This result is in agreement with the TGA analysis carried out to the microparticles, as observed in Figure 5, for thermal stability evaluation.

Figure 5 includes the TGA thermograms for Na-0.5Si and Na-0.25Si microparticles. The Na-0.5Si microparticles suffer a first weight loss at 135 °C (2.62 wt.%), which agrees with the endothermic peak observed in the DSC thermogram in Figure 3a and explained due to the presence of impurities of the synthesis of $NaNO_3$ microparticles. Additionally, a slight weight reduction is also produced at 295 °C (1.40 wt.%), which corresponds to the melting temperature of $NaNO_3$ in the microparticles determined by DSC (Tab. 1). Therefore, a decrease in the amount of $NaNO_3$ in Na-0.5Si microparticles is produced during melting, which may be due to the transformation into other compounds such as $NaNO_2$. Moreover, results obtained by

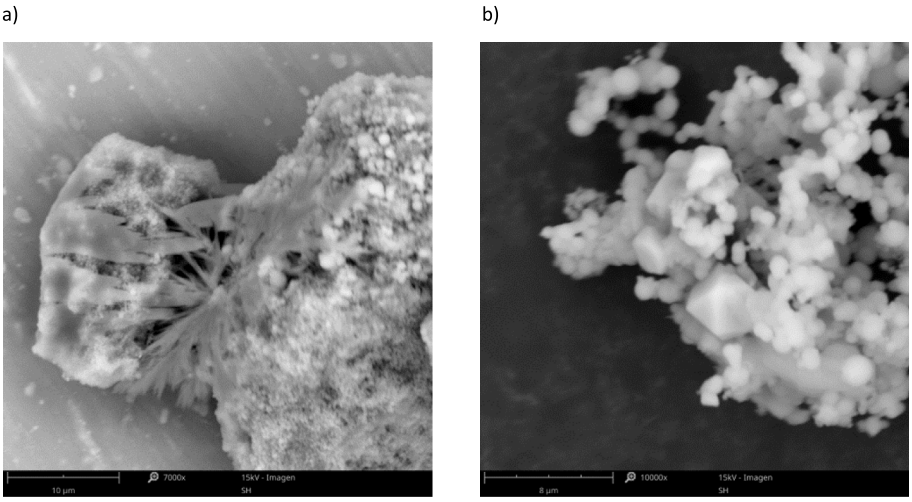

Fig. 6. SEM micrographs of (a) Na-0.5Si and (b) Na-0.25Si microparticles.

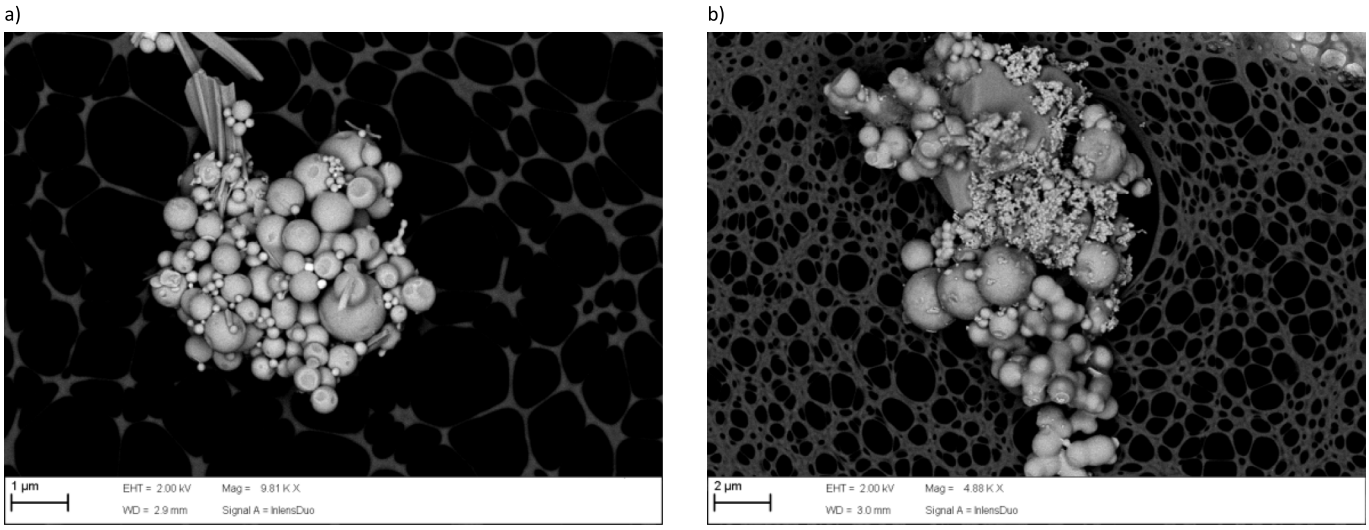

Fig. 7. FESEM micrographs of (a) Na-0.5Si and (b) Na-0.25Si microparticles.

DSC (Tab. 1) also show that the melting temperature of $NaNO_3$ in the Na-0.5Si microparticles has decreased respect to the raw $NaNO_3$. It is important to notice that the $NaNO_3$ weight loss has been produced in spite of the higher proportion of SiO_2 as shell material, compared to Na-0.25Si microparticles, which do not show any appreciable weight loss in the temperature range analyzed.

Figure 6 shows the morphology of the Na-0.5Si and Na-0.25Si microparticles obtained by SEM. As observed in Figure 6a for Na-0.5Si, $NaNO_3$ has crystallized as bundles coated with SiO_2 microparticles (wide particle size distribution: 0.2–0.5 µm), leading to $NaNO_3$ and SiO_2 composites. However, micrographs obtained for Na-0.25Si microparticles show prismatic shape $NaNO_3$ crystals coated with SiO_2 microspheres (particle size 0.5–1 µm), showing an entrapment of $NaNO_3$ crystals in SiO_2 microparticles agglomerates. Similar results have been obtained by using FESEM, as included in the micrographs in Figure 7. The different morphology of the $NaNO_3$ crystals may be explained due to the different crystal growth in the presence of different ratio of SiO_2 microparticles. Many studies in literature indicate that the crystal growth strongly depends on impurities and additives in the crystallization media or solution, affecting the composition, structure and final properties of the crystal [29]. The different morphology of the $NaNO_3$ particles leads to a different thermal behaviour, as previously observed by DSC and TGA, with better results for the Na-0.25Si microparticles, with the lower SiO_2 proportion.

Thermal stability of the Na-0.5Si and Na-0.25Si microparticles through thermal cycles has also been evaluated. Heating and cooling thermal cycles by DSC have been carried out from 50 to 400 °C and 400 to 50 °C at 10 °C/min. Melting and crystallization temperatures and enthalpies have been analyzed and included in Figure 8a and b, respectively for Na-0.5Si and Na-0.25Si and Table 2.

Data obtained for Na-0.5Si microparticles indicate that there is a loss of heating and cooling enthalpies with thermal cycles, i.e. 5.4 and 5.9 J/g, respectively, after 16 thermal cycles. This indicates a poor thermal stability of

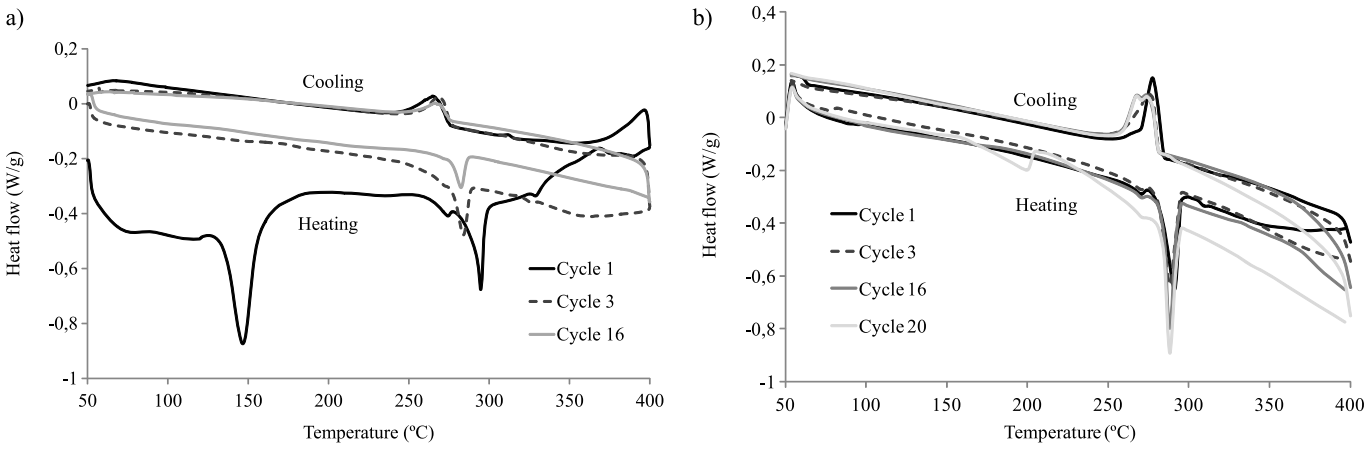

Fig. 8. DSC thermograms of thermal cycles for (a) Na-0.5Si and (b) Na-0.25Si microparticles.

Table 2. Melting and cooling temperatures (T_m, T_c) and enthalpies (ΔH_m, ΔH_c) during thermal cycles for Na-0.5Si and Na-0.25Si microparticles. Data obtained from DSC thermograms for heating and cooling processes.

Na-0.5Si	Heating		Cooling	
	T_m (°C)	ΔH_m (J/g)	T_c (°C)	ΔH_c (J/g)
Cycle 1	294.2	25.1	264.7	11.2
Cycle 2	283.7	10.9	268.8	10.7
Cycle 3	283.5	11.5	269.5	9.6
Cycle 16	282.3	5.4	266.3	5.9
Na-0.25Si	Heating		Cooling	
	T_m (°C)	ΔH_m (J/g)	T_c (°C)	ΔH_c (J/g)
Cycle 1	270.5; 293.9	26.2	281.0; 267.0	25.7
Cycle 2	270.5; 290.5	19.5	276.8; 267.5	21.5
Cycle 3	270.5; 288.2	20.0	275.1; 267.0	22.1
Cycle 16	270.5; 288.1	20.0	274.3; 270.5	22.0
Cycle 20	270.5; 288.2	21.9	274.8; 270.0	22.7

the Na-0.5Si microparticles, which agrees with the TGA results, showing a decrease in the amount of $NaNO_3$ in the microparticles, due to the gradual transformation of $NaNO_3$–$NaNO_2$ as observed with the continuous decrease in the melting temperature when increasing the number of thermal cycles ($NaNO_2$ melting temperature = 271 °C).

On the other hand, Na-0.25Si microparticles prepared with a lower proportion of SiO_2, show very good thermal stability even after 20 thermal cycles from 50 to 400 °C and 400 to 50 °C, with constant melting and cooling enthalpies (values higher than 20 and 22 J/g, respectively). Main melting and crystallization temperatures are around 288 °C and 275 °C, respectively (Tab. 2b). Moreover, it is important to notice in both the heating and cooling processes, the small peak, respectively at 270.5 °C and 267.0 °C. These peaks may correspond to the melting and crystallization of $NaNO_2$. The peak at 267.0 °C increases its intensity with thermal cycles, appearing as an intense crystallization peak at 270.5 °C in cycle 16. This could be explained due to the decomposition of $NaNO_3$ to $NaNO_2$ at the DSC temperature range to 400 °C. Commonly, $NaNO_3$ decomposition takes place at temperatures higher than 450 °C [30,31], therefore at 400 °C, a slow decomposition is produced, which gradually increases after each thermal cycle. As a difference, Na-0.5Si microparticles only show one melting and crystallization peak, which are shifted to lower melting temperatures and higher crystallization temperatures, respectively, when increasing thermal cycles. Na-0.5Si microparticles do not show the melting and crystallization peaks at 270.5 and 267.0 °C, as observed for the Na-0.25Si microparticles. Some authors have also shown the $NaNO_2$ formation when using $NaNO_3$ as PCM material [32]. Bauer et al. [33] have demonstrated that the presence of $NaNO_2$ in molten $NaNO_3$ leads to a reduction of the $NaNO_3$ melting temperature compared to raw $NaNO_3$. The thermal dissociation is reversible, which may explain the similar intensity of the melting peaks at 270.5 °C when increasing thermal cycles.

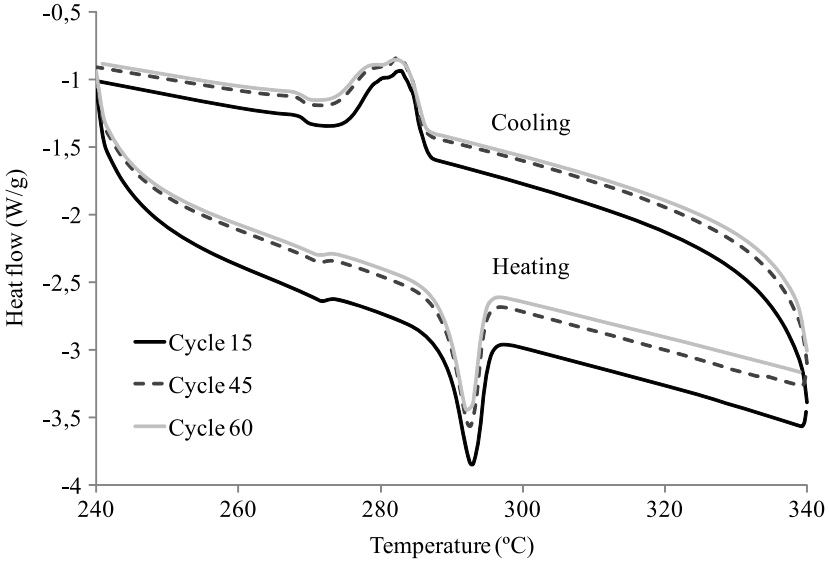

Fig. 9. DSC thermograms of thermal cycles in narrow temperature range (240–340 °C) for Na-0.25Si microparticles.

Table 3. Melting and cooling temperatures (T_m, T_c) and enthalpies (ΔH_m, ΔH_c) during thermal cycles in narrow temperature range (240–340 °C) for Na-0.25Si microparticles. Data obtained from DSC thermograms for heating and cooling processes.

Na-0.25Si	Heating		Cooling	
	T_m (°C)	ΔH_m (J/g)	T_c (°C)	ΔH_c (J/g)
Cycle 1	294.0	28.3	283.6	20.3
Cycle 15	292.0	26.8	282.8	26.3
Cycle 30	291.8	26.2	283.1	25.7
Cycle 45	291.7	26.3	282.2	25.3
Cycle 60	291.6	26.2	283.0	25.3

As also observed by these authors, the presence of NO_2^- in the $NaNO_3$ solution may lead to the changes in the $NaNO_3$ behaviour during melting and cristallyzation processes.

As previously observed in Figure 3 and Table 1, Na-0.25Si microparticles show higher TES capacity (higher melting and crystallization enthalpies) than the microparticles with the higher SiO_2 proportion (Na-0.5Si). This could be expected due to the lower amount of SiO_2 shielding the core $NaNO_3$. Moreover, and according to the TGA (Fig. 5) and DSC thermograms (Fig. 8, Tab. 2), the thermal stability through thermal cycles of Na-0.5Si microparticles is reduced compared to the microparticles prepared with lower SiO_2 ratio (Na-0.25Si). This is an unexpected result because of the higher amount of SiO_2 encapsulating and protecting the $NaNO_3$ used as PCM in the Na-0.5Si microparticles.

In real CSP applications, PCMs are not allowed to heat or cool after each thermal cycle in a wide range of temperature around its melting and crystallization temperature. To evaluate the TES capacity of Na-0.25Si microparticles when subjected to thermal cycles in narrower temperature ranges, DSC technique has also been used. Melting and crystallization enthalpies have been determined to analyze the $NaNO_3$ capacity to melt and crystallize in these narrow temperature ranges. Considering that the melting temperature of $NaNO_3$ in the microparticles is around 290 °C, thermal cycles between 240 and 340 °C have been carried out to Na-0.25Si microparticles (Fig. 9). Results included in Table 3 indicate the TES capacity of the encapsulated product even after 60 thermal cycles.

Results obtained with the thermal cycles in the temperature range between 240 and 340 °C indicate the TES capacity of $NaNO_3$ as PCM in the microparticles even after 60 thermal cycles, with constant melting and crystallization enthalpies higher than 26 and 25 J/g, respectively, as well as melting and crystallization temperatures (291.7, 283 °C, respectively). As a difference with the thermal cycles in Figure 8 (50–400 °C), in this case, for the 240–340 °C thermal cycles, the crystallization peak at 270 °C only appears as a shoulder of the main crystallization peak at around 283 °C. This may be explained due to the lower maximum temperature applied, 340 °C, avoiding the transformation of $NaNO_3$–$NaNO_2$, previously observed in the thermal cycles carried out to 400 °C.

Hence, the effectiveness of $NaNO_3$ microparticles to be used as PCMs is determined by the maximum temperature during use. Temperatures higher than 400 °C slightly lead to the formation of $NaNO_2$ and therefore, modifications on the melting and crystallization temperatures and enthalpies respect to the raw $NaNO_3$.

4 Conclusions

Sol–gel has been demonstrated as a feasible technology for the microencapsulation of $NaNO_3$ using SiO_2 as shell material.

Effectiveness of microencapsulated $NaNO_3$ as TES material greatly depends on the morphology of microparticles and therefore, on the $NaNO_3$:SiO_2 ratio. Results have shown that Na-0.25Si microparticles have higher energy storage capacity even with a lower proportion of SiO_2 respect to the $NaNO_3$ core material compared with the higher ratio in Na-0.5Si microparticles. The SiO_2 shell may affect the $NaNO_3$ crystal growth. This indicates the great influence of experimental parameters on the effectiveness of microencapsulated materials. In this sense, deeper work is being done by the authors to analyze the influence of the $NaNO_3$ crystal phase on its energy storage capacity when microencapsulated within SiO_2 shells.

TES stability of microencapsulated $NaNO_3$ with SiO_2 depends among other factors on the maximum temperature during use. Temperatures higher than 400 °C lead to the dissociation of NO_3^- to NO_2^- and therefore to a modification of the TES properties of $NaNO_3$.

The authors gratefully acknowledge the financial support received from European Commission and Romanian Government-Management Authority from Ministry of Research and Innovation, in the frame of Competiveness Operational Programme, Action A1.1.4-E-2015, project ID P_37_776, SMIS code 104730, Acronym ENERHIGH.
Albert Ioan Tudor also gratefully acknowledges the financial support received from Romanian Ministry of Research and Innovation in the frame of the project PN 16 20 0302.

References

1. A. Gil, M. Medrano, I. Martorell, A. Lázaro, P. Dolado, B. Zalba, L.F. Cabeza, State of the art on high temperature thermal energy storage for power generation. Part 1-concepts, materials and modellization, Renew. Sustain. Energy Rev. **14** (2010) 31–55
2. M. Medrano, A. Gil, I. Martorell, X. Potau, L.F. Cabeza, State of the art on high-temperature thermal energy storage for power generation. Part 2-case studies, Renew. Sustain. Energy Rev. **14** (2010) 56–72
3. S. Bellan, A. Cordiviola, S. Barberis, A. Traverso, J. González-Aguilar, M. Romero, Numerical analysis of latent heat storage system with encapsulated phase change material in spherical capsules, Renew. Energy Environ. Sustain. **2** (2017) 3
4. M. Graham, E. Shchukina, P. Felix De Castro, D. Shchukin, Nanocapsules containing salt hydrate phase change materials for thermal energy storage, J. Mater. Chem. A **4** (2016) 16906–16912
5. D. Platte, U. Helbig, R. Houbertz, G. Sextl, Microencapsulation of salt hydrate melts for phase change applications by surface thiol-michael addition polymerization, Macromol. Mater. Eng. **298** (2013) 67–77
6. F. Salaun, E. Devaux, S. Bourbigot, P. Rumeau, Influence of the solvent on the microencapsulation of a hydrated salt, Carbohydr. Polym. **79** (2010) 964–974
7. EP 2015 2 119 498 A1, Procedure for microencapsulation of phase change materials by spray-drying
8. S. Ushak, M.J. Cruz, L.F. Cabeza, M. Grágeda, Preparation and characterization of inorganic PCM microcapsules by fluidized bed method, Materials **9** (2016) 24
9. W. Su, J. Darkwa, G. Kokogiannakis, Development of microencapsulated phase change material for solar thermal energy storage, Appl. Therm. Eng. **112** (2017) 1205–1212
10. US 2011/0259544, Encapsulated phase change apparatus for thermal energy storage
11. US 2012/0055661, High temperature thermal energy storage system
12. US 2015/0284616, Encapsulation of thermal energy storage media
13. N. Maruoka, T. Akiyama, Thermal stress analysis of PCM encapsulation for heat recovery of high temperature waste heat. J. Chem. Eng. Jpn **36** (2003) 794–798
14. Y. Hong, S. Ding, W. Wu, J. Hu, A.A. Voevodin, L. Gschwender, Ed. Snyder, L. Chow, M. Su, Enhancing heat capacity of colloidal suspension using nanoscale encapsulated phase-change materials for heat transfer, Appl. Mater. Interfaces **2** (2010)
15. P. Chou, C. Chandrasekaran, G.Z. Cao, Sol–gel derived hybrid coatings for corrosion protection, J. Sol–Gel Sci. Technol. **26** (2003) 321–327
16. R.B. Figueira, C.J.R. Silva, E.V. Pereira, Organic-inorganic hybrid sol–gel coatings for metal corrosion protection: a review of recent progress, J. Coat. Technol. Res. **12** (2015) 1–35
17. M. Liu, W. Saman, F. Bruno, Review on storage materials and thermal performance enhancement techniques for high temperature phase change thermal storage systems, Renew. Sustain. Energy Rev. **16** (2012) 2118–2132
18. B. Zalba, J.M. Marin, L.F. Cabeza, H. Mehling, Review on thermal energy storage with phase change: materials, heat transfer analysis and applications, Appl. Therm. Eng. **23** (2003) 251–283
19. S. Kuravi, J. Trahan, D. Yogi Goswami, M.M. Rahman, E.K. Stefanakos, Review thermal energy storage technologies and systems for concentrating solar power plants, Prog. Energy Combust. Sci. **39** (2013) 285–319
20. M.M. Kenisarin, High-temperature phase change materials for thermal energy storage, Renew. Sustain. Energy Rev. **14** (2010) 955–970
21. J.C. Gomez, N. Calvet, A.K. Starace, G.C. Glatzmaier, Ca $(NO_3)_2$-$NaNO_3$-KNO_3 Molten Salt Mixtures for Direct Thermal Energy Storage Systems in Parabolic Trough Plants, J. Sol. Energy Eng. **135** (2013)
22. Y. Zheng, W. Zhao, J.C. Sabol, K. Tuzla, S. Neti, A. Oztekin, J.C. Chen, Encapsulated phase change materials for energy storage − characterization by calorimetry, Sol. Energy **87** (2013) 117–126
23. T. Vijay Kumar, A. Sadananda Chary, A.M. Awasthi, S. Bhardwaj, S. Narender Reddy, Effect of nano SiO_2 on properties of structural, thermal and ionic conductivity of 85.32 $[NaNO_3]$–14.68$[Sr(NO_3)_2]$ mixed system, Ionics **21** (2015) 1341–1349

24. T. Jriri, J. Rogez, C. Bergman, J.C. Mathieu, Thermodynamic study of the condensed phases of $NaNO_3$, KNO_3 and $CsNO_3$ and their transitions, Thermochim. Acta, **266** (1995) 147–161
25. T. Bauer, D. Laing, R. Tamme, Characterization of sodium nitrate as phase change material, Int. J. Thermophys. **33** (2012) 91–104
26. C. Alba-Simionesco, B. Coasne, G. Dosseh, G. Dudziak, K.E. Gubbins, R. Radhakrishnan, M. Sliwinska-Bartkowiak, Effects of confinement on freezing and melting, J. Phys.: Condens. Matter. **18** (2006) 15–68
27. M. Fuensanta, U. Paiphansiri, M.D. Romero-Sánchez, C. Guillem, Á.M. López-Buendía, K. Landfester, Thermal properties of a novel nanoencapsulated phase change material for thermal energy storage, Thermochim. Acta **565** (2013) 95–101
28. Q. Guo, T. Wang, Preparation and characterization of sodium sulfate/silica composite as a shape-stabilized phase change material by sol–gel method, Chin. J. Chem. Eng. **22** (2014) 360–364
29. R. Benages Vilau, Growth, Morphology and solid state miscibility of alkali nitrates, Doctoral Thesis, University of Barcelona, 2013
30. Y. Hoshino, T. Utsunomiya, O. Abe, The thermal decomposition of sodium nitrate and the effects of several oxides on the decomposition, Bull. Chem. Soc. Jpn. **54** (1981) 1385–1391
31. P. Gimenez, S. Fereres, Effect of heating rates and composition on the thermal decomposition of nitrate based molten salts, Energy Procedia **69** (2015) 654–662
32. R.W. Bradshaw, N.P. Siegel, Molten nitrate salt development for thermal energy storage in parabolic trough solar power systems, in: Proceedings of ES2008-54174. Energy Sustainability 2008 August 10–14, Jacksonville, Florida USA, 2008
33. T. Bauer, D. Laing, U. Kröner, R. Tamme, The 11th International Conference on Thermal Energy Storage – Effstock in Stockholm, Sweden, 2009

Cite this article as: Maria Dolores Romero-Sanchez, Radu-Robert Piticescu, Adrian Mihail Motoc, Francisca Aran-Ais, Albert Ioan Tudor, Green chemistry solutions for sol–gel micro-encapsulation of phase change materials for high-temperature thermal energy storage, Manufacturing Rev. **5**, 8 (2018)